Matrix atomic losses and oxygen incorporation under ruby-laser irradiation of silicon in gaseous atmospheres

M. Berti, L. F. Doná dalle Rose, and A. V. Drigo
Dipartimento di Fisica "Galileo Galilei" Università degli Studi di Padova, via Marzolo 8, I-35131 Padova, Italy and Consorzio Interuniversitario di Struttura della Materia (CISM) del Ministero della Pubblica Istruzione, I-35131 Padova, Italy

C. Cohen and J. Siejka
Groupe de Physique des Solides de l'Ecole Normale Supérieure, Université de Paris VII, Tour 23, 2 place Jussieu, 75251 Paris Cédex 05, France

G. G. Bentini
Istituto Laboratorio di Chimica e Tecnologia dei Material per l'Elettronica del Consiglio Nazionale delle Ricerche, via Castagnoli 1, I-40126 Bologna, Italy

E. Jannitti
Centro dei Gas Ionizzati del Consiglio Nazionale delle Ricerche, via Gradenigo 8, I-35100 Padova, Italy
(Received 3 February 1986)

The present work provides information both on the loss and the incorporation mechanisms which occur in silicon during high-fluence pulsed-laser irradiation in different gas atmospheres. ⟨100⟩ silicon samples were irradiated with 20-ns single pulses from a *Q*-switched ruby laser in O_2, CO_2, N_2, and Ar atmospheres at different ambient pressures. Under these conditions and at sufficiently high laser fluences, significant impurity incorporation may take place, competing with important material loss. Incorporation is observed only for those gaseous atmospheres which lead to a chemical reaction at the surface of the molten silicon. A comparison between heat-flow-model calculations and experimental results seems to indicate that the material-loss mechanism proceeds via a thermodynamical evaporation rather than via a boiling process. Moreover, the observed results exclude an incorporation mechanism taking place via a reaction of the evaporated atoms with the ambient gas, followed by deposition on the sample surface, and rather suggest the occurrence of a reaction at the molten surface. Convective transport is then assumed in order to explain the very quick and massive incorporation. Finally, a simple phenomenological model, which describes the material loss and the impurity-incorporation process, is presented. The model is successfully used to fit the experimental data concerning O_2- and CO_2-gas atmospheres.

I. INTRODUCTION

In the past few years, an increasing number of works have been devoted to the study of pulsed-laser-induced reactions between the irradiated surface and the environment.[1–4] At high laser fluences the thermal excitation of the solids is the most important process; the heating results from a number of phenomena including nonradiative recombination and energy transfer from hot electrons. In particular, for semiconductors, the thermal excitation gives rise to several effects such as free carrier generation, surface melting, evaporation, etc., all of which are important for surface reactions. Some experiments[3,5] deal with relatively low laser-energy densities; in these experiments the surface temperature is not far from the melting point of the material, so that only a thin surface layer is molten and the material loss by evaporation is limited to less than one monolayer[6] and evaporation does not significantly affect the process. Under these conditions the incorporation from the external environment proceeds in the liquid phase at relatively low speed (even if it is much higher than in the solid phase) so that several irradiations are necessary to produce an appreciable reacted layer.

Some experiments[1,2,4,7] have been devoted to irradiation at high energy densities; in these conditions the surface is heated at temperatures well above melting point and a massive incorporation from the gaseous environment takes place. Moreover, because of the very high surface temperature reached during irradiation, material losses by evaporation or boiling are expected. The overall process is very complex as it includes adsorption, chemical reactions, loss of atoms, diffusion, etc., and at present no detailed modelization of the phenomenon has yet been presented.

In the present work we report the results of a series of *ad hoc* experiments performed to obtain some information on the loss and gain mechanism involved as a consequence of the irradiation of silicon in oxidizing atmosphere. The experimental results have been analyzed by taking into account the temperature transients in the surface region as computed by solving the one-dimensional heat-flow equation.[8] Particular emphasis is devoted to the description of the material loss and to the oxygen-transport mechanisms.

 ©1986 The American Physical Society

As to the first point, some authors[9] have assumed that material loss could take place by some particular mechanisms such as liquid-droplet ejection; an alternative possibility is the loss of material by boiling of the molten layer but other authors[6] seem to conclude that this mechanism cannot take place during thermal transients which are extremely quick and which produce very shallow molten regions.

The experiments reported in the present paper more simply suggest that, in our fluence range, only thermodynamical evaporation takes place at the surface, while the ordinary boiling process seems to be excluded. As a consequence the molten surface reaches very high superheating temperatures.

As to the observed massive oxygen incorporation in silicon, two possible mechanisms are discussed, i.e., reaction in the gas phase between the evaporated material and the reactive atmosphere followed by redeposition of the oxide on the surface, and reaction in the molten phase. The experiments reported here exclude the former process; a very efficient transport mechanism is then required in order to explain why the observed massive oxygen incorporation may take place in the very short characteristic times of the transients. We give evidence for this material transport and show that simple diffusion is not sufficient: convective processes have to be considered. Finally, we extend our experiments and interpretation to the reaction with gases other than O_2, with particular emphasis on CO_2.

II. EXPERIMENTAL

The samples used for the present work were $\langle 100 \rangle n$-type doped Si($1-4$ Ω cm) wafers. To observe the effects due to the initial surface conditions different cleaning procedures of the samples were used: in most cases the native oxides were simply dissolved by chemical etch just before the laser irradiation; in some other cases the native oxide on Si samples was etched in concentrated HF acid and the samples were extracted from the bath through a surface floating layer of C_6H_5Br. This method[10] has been proved to give stable and minimum coverages of about ($1-3\times 10^{15}$ O atoms/cm^2 (i.e., 0.5—1 monolayer); in other cases the native oxide was left on the surface.

In order to get more insight into the oxygen motion and the mechanism of oxygen gain and loss under laser treatment, tracing experiments were performed. To this purpose some ^{18}O enriched anodic oxides with thicknesses ranging from 7 to 70 nm were anodically grown on the silicon samples. Moreover, layered structures of ^{18}O and ^{16}O oxides were grown by subsequent thermal oxidations in ^{16}O then in ^{18}O dry atmosphere. Owing to the oxidation mechanism (long-range oxygen migration) this procedure leads to the formation of a ^{18}O oxide layer at the Si interface with a very uniform thickness, topped by a ^{16}O surface oxide.[11]

The samples were laser irradiated in a cell connected to a rough pump and to a series of gas bottles (see Fig. 1). After the introduction of the sample, the cell was evacuated by the rough pump ($P\approx 10^{-2}$ Torr), then the cell was filled with a gas up to the required pressure. The pressure was measured by a Hg manometer up to 8 atm. The gases used in the present investigation were N_2, O_2, CO_2, and Ar. The laser light entered the cell through a 4-mm-thick quartz window.

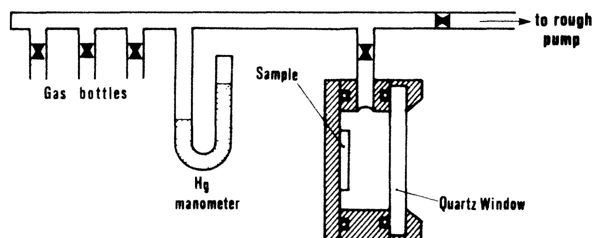

FIG. 1. Schematic drawing of the experimental arrangement. The laser light enters the cell from the right-hand side of the figure.

Laser irradiations were performed at the Centro Gas Ionizzati of the Consiglio Nazionale delle Ricerche (CNR) in Padova by using a Q-switched ruby laser ($\lambda=0.69$ μm, $\tau=20$ ns). In all cases the samples were irradiated with a single pulse. In order to increase the energy density, a convergent lens (focal length 1 m) was used to reduce the beam diameter from 2 cm to a few mm at the surface of an emery polished glass plate acting as beam homogenizer. Then the divergent beam entered into the cell striking onto the sample (see Fig. 2). For a given geometry the energy density at the sample surface was varied by changing the laser parameters. By substituting the sample with a calorimeter, a calibration curve of the energy density was systematically established. The accuracy of such a calibration was repeatedly checked for many laser shots and for different geometries, both before and after an irradiation run. An overall accuracy of about 5% is maintained over a period of several hours. The overall uniformity of the beam at the sample surface was checked by measuring the energy arriving into the calorimeter after passing through diaphragms of different diameter. This control was performed for many different energy densities. It was found that, within a diameter of 6 mm, the average beam homogeneity was always better than several percent.

The irradiated samples were analyzed by means of nuclear microanalysis with the 2-MV Van der Graaff facilities of both the Ecole Normale Supérieure (Paris) and the Laboratori Nazionali di Legnaro (Padova). Rutherford backscattering (RBS) of 1.8 MeV ^{4}He in channeling geometry was used to study the composition of the sur-

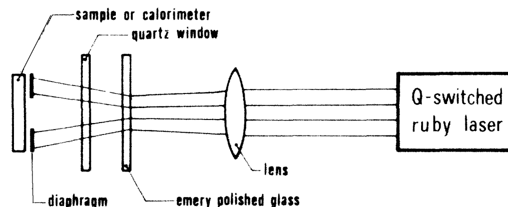

FIG. 2. Schematic of laser-irradiation geometry and fluence calibration.

face layers, whereas the $^{16}O(d,p)^{17}O$, $^{18}O(p,\alpha)^{15}N$, $^{14}N(d,p_5)^{15}N$, and $^{12}C(d,p)^{13}C$ nuclear reactions were used to accurately measure the absolute amount of the different elements incorporated in the near surface layer of the samples. Moreover, the narrow resonance at 629 keV of the $^{18}O(p,\alpha)^{15}N$ nuclear reaction was used to determine the ^{18}O depth profile, by recording excitation curves. The nuclear microanalysis experiments were calibrated by means of different absolute standards with an accuracy of 3%.

III. RESULTS

A. Irradiation under $^{16}O_2$ atmosphere

The amount of oxygen, as measured by the $^{16}O(d,p)^{17}O^*$ nuclear reaction, at the surface of Si samples irradiated in 4 atm O_2, is reported in Fig. 3 as a function of the laser-pulse energy density. The main feature of this figure is the very sharp increase of the oxygen content around 3 J/cm^2 followed by a nearly constant value for higher energy densities. We can say that there is a threshold fluence of 3.1 ± 0.2 J/cm^2 for the incorporation of a significant amount of oxygen by single-pulse laser irradiation. The same threshold was found for different O_2 pressures whereas the amount of oxygen for irradiations at fluences above the threshold appears to depend on the oxygen pressure.

Figure 4 shows the amount of oxygen incorporated at an energy density of 3.5 ± 0.2 J/cm^2 as a function of the O_2 pressure. The oxygen incorporation is roughly linear at low pressures and saturates at higher pressures.

The most striking feature of all these data is the threshold which is much higher than the fluence required to melt Si or SiO_2. A similar behavior (i.e., a threshold for oxygen incorporation much higher than the melting fluence) has been found in the case of laser irradiation of GaAs.[4] The threshold in that case was connected to the removal of the native oxide due to the volatile properties of As_2O_3. For this reason the experiments on Si were repeated with different surface cleaning methods (as reported in Sec. II), in order to minimize the surface oxide. The results for different sets of samples are also reported in Fig. 3; they show the same behavior as the samples covered by native oxide so that the threshold fluence seems not to be related to the native oxide-layer thickness.

The total oxygen content, as measured by means of the $^{16}O(d,p)^{17}O$ nuclear reaction, does not give any information about the composition ratio of the final compounds. To overcome this ambiguity some significant samples were analyzed with RBS technique both in channeling and in random geometries. Figure 5 shows that the heights of the surface peaks concerning oxygen and silicon in a RBS-channeling spectrum, recorded on a laser irradiated sample, agree with the corresponding plateau heights measured on a thermally oxidized silicon sample, thus indicating that the final result of the oxygen incorporation is the formation of a SiO_2 layer at the surface region. Such nearly stoichiometric oxygen-versus-silicon composition ratio was always observed by comparing the oxygen and silicon peak integrals.

In order to investigate better the incorporation and transport mechanism of oxygen and to discriminate between incorporation and loss processes, a set of wafers was covered by a 7-nm-thick layer of anodic oxide, which was ^{18}O enriched ($\approx 50\%$). Part of these samples were ir-

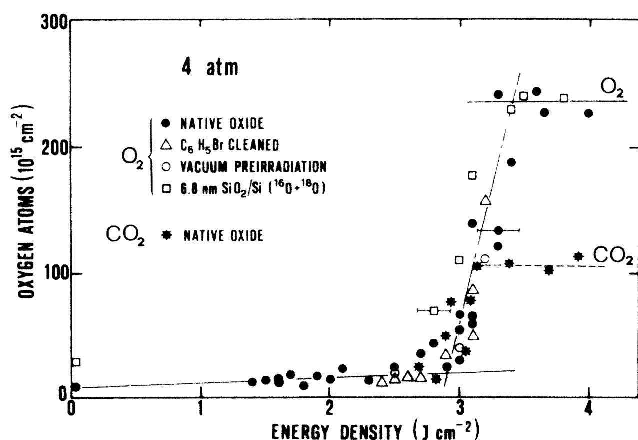

FIG. 3. Total ^{16}O content measured by means of $^{16}O(d,p)^{17}O^*$ nuclear reaction. Results from single-pulse irradiations at 4-atm O_2 and CO_2 are reported as a function of pulse-energy densities. The initial cleaning conditions are displayed by different symbols (see inset). The amount of ^{16}O measured in virgin samples is also reported. The indetermination on the energy density is given by the error bars whereas that of the oxygen content is within the point dimensions.

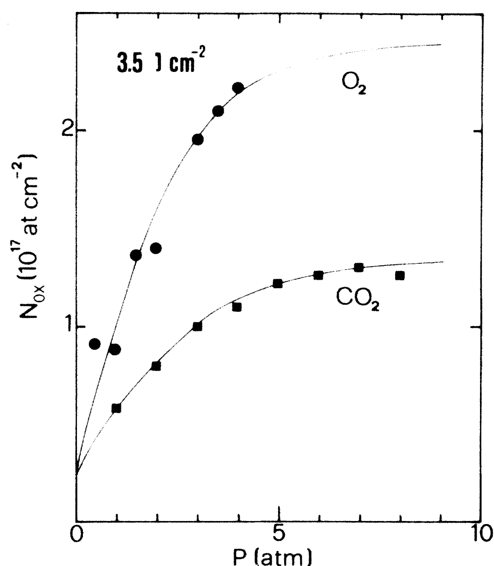

FIG. 4. Amount of oxygen incorporated at an energy density of (3.5 ± 0.2) J/cm^2 as a function of pressure for O_2 and CO_2 atmosphere. Full lines are the best fits computed by means of the phenomenological model described in the text; experimental data: $x_0=25\times10^{15}$ atoms/cm^2, $x_s=245\times10^{15}$ atoms/cm^2 (O_2), $x_s=135\times10^{15}$ atoms/cm^2 (CO_2); fitting parameter: $t_{max}=148$ ns.

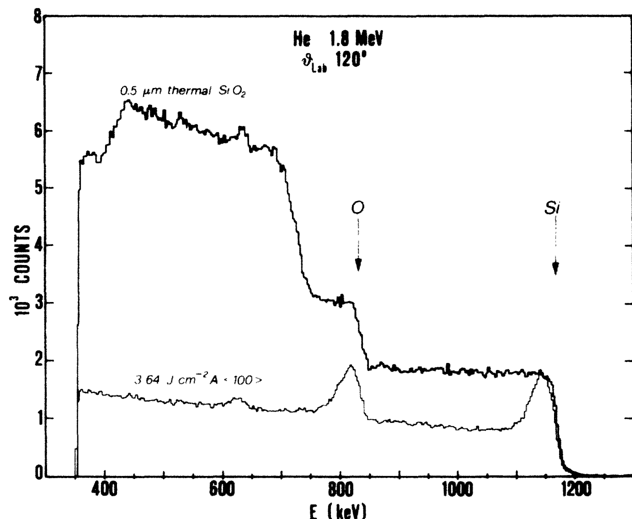

FIG. 5. RBS channeling spectrum of a thermally oxidized silicon sample superposed to the channeling spectrum of a sample irradiated at 4-atm O_2 at an energy fluence of 3.64 J/cm^2. 2.8 keV/channel. Arrows indicate the surface scattering energies for Si and O.

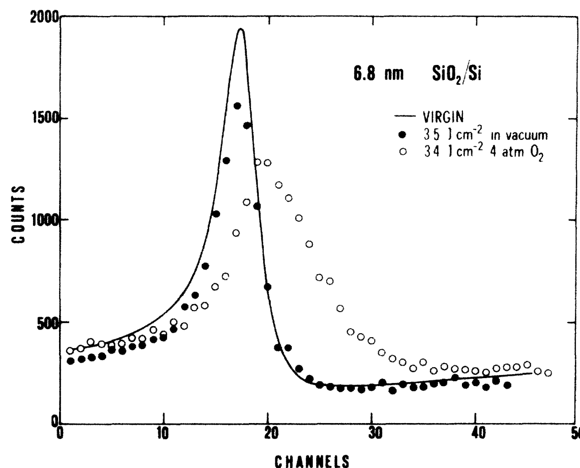

FIG. 6. $^{18}O(p,\alpha)^{15}N$ excitation curves on 6.8-nm oxide-covered samples irradiated in different conditions: ●, 3.5 J/cm^2 in vacuum; ○, 3.4 J/cm^2 in 4-atm O_2. The excitation curve of the unirradiated sample (virgin) is shown by the continuous line for comparison. 0.4 keV/channel.

radiated in vacuum at energy densities both below and above the threshold and all showed only a very small ^{18}O loss corresponding to about 5–10% of the initial value. Moreover, the oxygen profile measured by means of the $^{18}O(p,\alpha)^{15}N$ resonant nuclear reaction did not change appreciably even after irradiation above the threshold as shown by the excitation curves of Fig. 6. Another part of these oxidized samples was irradiated at a pressure of 4 atm of oxygen. In this case no ^{18}O loss was observed at all, whereas ^{16}O incorporation was evident after irradiation at fluences above the threshold (see Fig. 3). The ^{18}O excitation curve of a sample irradiated at 3.4 J/cm^2 is also shown in Fig. 6. This curve corresponds to a quasi uniform ^{18}O distribution over a 50-nm-thick SiO_2 layer. On the other hand, it should be noticed that the total amount of oxygen in this sample is 230×10^{15} atoms/cm^2 corresponding again to about 50 nm of SiO_2.

These ^{18}O experiments indicate that the cleanliness of the surface does not influence the oxygen uptake and that the surface oxide is dissolved or transported inside the melted layer. As the final result is the formation of a uniform SiO_2 surface layer, some kind of oxygen segregation must occur later, during the resolidification. The negligible oxygen loss evidenced by thin films, even when irradiated at energy densities above 3 J/cm^2 seems to be in contrast with the thermal transient computations (see Sec. IV) which indicate that appreciable evaporation should take place under these conditions.

In order to better investigate this point, samples with thicker ^{18}O-enriched anodic oxide layers (41 and 69 nm) were prepared and then irradiated at 3.5 J/cm^2 in O_2 at 4 atm. The amounts of ^{16}O and ^{18}O before and after irradiation are reported in Table I. From these data it appears that oxygen loss does occur if the oxide is thicker than 7 nm. On the other hand, the total oxygen content after irradiation in an oxidizing atmosphere is always equivalent to about 50 nm of SiO_2.

In a further experiment a layered $Si\,^{16}O_2/Si\,^{18}O_2/Si$ sample, prepared by thermal oxidation as described in Sec. II, was irradiated at an energy density of 3.85 J/cm^2 at 4 atm in $^{16}O_2$ ambient. The initial structure was a sandwich of 41 nm $Si^{16}O_2$ followed by 15 nm $Si\,^{18}O_2$ (99% enrichment). The most striking result of the irradiation is a strong (40%) ^{18}O loss. In this case again the residual ^{18}O

TABLE I. ^{16}O and ^{18}O content of samples covered by ^{18}O-enriched anodic oxide layers of different initial thickness, as measured *before* and *after* irradiation at 3.5 J/cm^2 in an O_2 atmosphere at 4 atm. The quantity Δ represents the difference between *after* and *before* content. Units are in 10^{15} atoms/cm^2. The molecular density of the oxide has been assumed to be 2.2×10^{22} SiO_2/cm^3.

Initial oxide thickness (nm)	^{16}O Before	^{16}O After	^{16}O Δ	^{18}O Before	^{18}O After	^{18}O Δ	$^{16}O+^{18}O$ Before	$^{16}O+^{18}O$ After	$^{16}O+^{18}O$ Δ	Final oxide thickness (nm)
6.8	15	215	+200	15	15		30	230	+200	52
41	108	204	+96	73	32	−41	181	236	+55	54
69	146	178	+32	159	50	−109	305	228	−77	52

is uniformly distributed over the final oxide layer.

Some important conclusions can be drawn from the results on ^{18}O contents and concentration profiles after irradiation:

(i) Whatever the initial oxide thicknesses and ^{18}O profiles are, the isotope ^{18}O is uniformly distributed into the oxide film after irradiation. This implies that atomic mass transport takes place. However, the only information about concentration profiles does not tell us if such uniform mixing takes place at the beginning of the process or during resolidification.

(ii) No ^{18}O loss is observed in thin films whereas strong losses are seen for thick oxides, and this even for a sample on which ^{18}O is initially buried 41 nm below the surface. This implies that the transport is already efficient in the very short time where losses may occur by evaporation. The transport dilutes the thin oxide films into the melted bulk and prevents their evaporation. For thicker films the dilution is not sufficient and some oxygen evaporation takes place. Symmetrically, the transport mechanism drives part of the buried ^{18}O of the layered oxide in the surface region very quickly, thus explaining the ^{18}O loss in this case.

B. Irradiation in different atmospheres

Irradiations of Si samples have been performed in other ambient atmospheres: Ar, N_2, NH_3, and CO_2. The results are reported in detail in Ref. 12. The main conclusion is that when the chemical reaction between Si and a gas molecule is not energetically favored no incorporation is observed at the end of the process. This is, for instance, the case for irradiations in Ar or N_2 atmospheres (the former being a noble gas, the latter having a rather strong molecular bond). We will focus here on the CO_2 case.

For this molecule the reaction

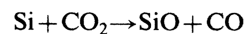

$$Si + CO_2 \rightarrow SiO + CO$$

FIG. 7. Optical micrographs of the surface of some selected samples. (a) and (b), 7-nm SiO_2 on Si after 2.3 and 3.5 J/cm^2 irradiation in vaccum, respectively; (c) and (d), Si irradiated at 3.5 J/cm^2 under 2 atm of NH_3 and 4 atm of O_2, respectively.

is energetically favored, while any reaction between Si and CO is not possible, again because the CO molecular bond is too strong.

In this situation we observe a strong oxygen incorporation above the same fluence threshold as for the O_2 atmosphere (see Fig. 3). However, for a given gas pressure the oxygen incorporation for O_2 is nearly double than for CO_2. The dependence of the oxygen incorporation on the gas pressure is shown in Fig. 4 together with the O_2 data. In both cases the incorporation saturates above about 5 atm, the saturation value being again double for O_2 than for CO_2.

The carbon contamination of the oxide films formed in CO_2 is rather small ($\approx 10^{16}$ C atoms/cm^2) confirming that, even though some nonreacting CO molecules were incorporated in the molten phase, they are later expelled at some step of the process.

C. Surface roughness

Below the energy threshold for incorporation (i.e., 3 J/cm^2) the surface roughness is low, even for irradiated samples preoxidized over ≈ 10 nm [see Fig. 7(a)]. On the contrary, above 3 J/cm^2, very high surface roughness is observed, as illustrated in Figs. 7(b)–7(d). The surface morphology seems to be characterized by swollen areas of $\approx 50\ \mu m^2$ and associated thicknesses on the order of 1 μm. A striking feature is that this morphology does not depend markedly on the ambient, under which irradiation takes place, and on the final incorporation, as it can be seen by comparing Figs. 7(b)–7(d) referring to irradiations under vacuum, NH_3, and O_2 ambient, respectively.

We insist on the fact that, even though their surface morphology is very rough, the samples in which incorporation takes place do form nearly uniform and continuous surface oxide films. This is unquestionably demonstrated by the channeling RBS spectrum of Fig. 5, where no marked tail is observed on the Si and O signals (notice that this spectrum has been recorded at a scattering angle $\theta_{lab} = 120°$ and should consequently be highly sensitive to nonuniformities in the oxide thicknesses). It is also proved by the uniform oxygen profiles extracted from the excitation curves of Fig. 6. Our interpretation for the observed surface roughness will be given in Sec. V.

IV. HEAT-FLOW CALCULATION

In order to interpret the experimental results and to discuss the occurrence and the relative importance of different possible physical mechanisms, it is useful to have a description of the main features of the laser-induced thermal transients in the irradiated samples. This may be easily accomplished by means of a heat-flow-model calculation[13,14] simply based on the heat-diffusion equation.

We have performed the heat-flow calculations according to the usual schemes[15] based on the numerical integration of the one-dimensional heat-flow equation, subjected to appropriate boundary conditions at the surface (no radiative loss), in the very deep bulk (temperature equal to room temperature) and at the interfaces where the phase transitions occur (i.e., at the liquid-solid interface, where melting or resolidification occur, and at the surface, when its temperature allows evaporation or boiling). While the boundary conditions appropriate to melting and resolidification have been discussed in many papers,[8,13] little attention has been paid, up to now, to the surface boundary conditions, when material loss occurs. If the surface instantaneous position, with respect to a reference frame fixed in the bulk of the sample, is denoted by $S = S(t)$, then the following Stefan condition (i.e., a moving-boundary condition) applies,[16] as a substitute for the more usual condition of no radiative loss

$$\rho_L H_{\text{vap}} \dot{S} = K_L \left. \frac{\partial T}{\partial x} \right|_{x=S^+}, \tag{1}$$

where ρ_L, H_{vap}, and K_L are, in order, the density, the (temperature-independent) latent heat of vaporization, and the thermal conductivity in the liquid phase; $\dot{S}$ is the surface front velocity and it is determined according to the loss mechanism to be modeled. In principle, two different physical processes may occur, depending on the times involved and on the pressure conditions. The first mechanism, to which we shall refer as "thermodynamical surface vaporization," implies an evaporation rate which is simply governed by the surface temperature, let it be T_s, according to

$$\dot{S} = U \exp(-M H_{\text{vap}} / k_B T_s), \tag{2}$$

where M is the vaporizing species molecular (atomic) mass, k_B the Boltzmann constant, and

$$U = P_0 \exp(M H_{\text{vap}} / k_B T_b) / \rho_L \sqrt{2\pi k_B T_s / M},$$

P_0 and T_b being, respectively, the boiling pressure and temperature in standard conditions. This process occurs at any temperature above melting and it may be the only one existing under conditions which prevent boiling of the molten pool. The only practical limit to the maximum temperature attainable is then the liquid critical temperature[17] and the quantity $\rho_L \dot{S}$ represents the maximum vaporizing flux at a given surface temperature.

The second possible process is the boiling of the molten layer. In this case, once the molten sample has attained boiling temperature, all or part of the excess heat deposited in the near-surface region may go into boiled-off material, because of some mechanism which enhances the actual evaporating surface (e.g., vapor bubble nucleation in the bulk molten liquid, convective motions, etc.) This second process can be modeled by assuming

$$\dot{S} = \begin{cases} U \exp(-M H_{\text{vap}} / k_B T_s), & \text{when } T_s < T_b \\ \text{as given by the heat-flow equation} & \\ \text{plus the boundary condition} & \\ \text{for the heat flux at the surface,} & \\ \text{i.e., } \Phi_s = \rho_L H_{\text{vap}} \dot{S} \text{ (see the Appendix),} & \\ \text{when } T_s = T_b\,. & \end{cases} \tag{3}$$

It is impossible to discriminate *a priori* between surface evaporation and boiling processes; as a consequence we performed the calculation for both processes and com-

TABLE II. Main computed properties of the thermal transient induced by a 20-ns ruby laser pulse at the energy densities E_p shown in the first line. Each of the columns referring to a given energy density exhibits the property values as computed within both the *thermodynamical surface evaporation* (first value) and the *boiling* (second value) model. The boiling temperature corresponds to an ambient pressure of 4 atm.

Property \ E_p (J/cm^2) / Absorbed energy (J/cm^2)	2.5 / 1.14		3.0 / 1.29		3.5 / 1.44		4.0 / 1.59	
Maximum surface temperature (°C)	3049	3049	3825	3690	4511	3690	5153	3690
Duration of the molten phase at the surface (ns)	365	365	518	500	>700	529	792	542
Maximum molten depth (nm)	731	731	952	944	1130	976	1255	990
Resolidification velocity (m/s)	1.90	1.90	1.70	1.77	1.58	1.63	1.48	1.58
Silicon loss (nm)			0.9	3.5	5.1	31.3	15.1	63.9
Duration of the loss process (ns)			14	4	21	12	24	14
$\vert \partial T/\partial x \vert_{max}$ (10^7 K/cm)	5.4	5.4	6.7	8.2	8.4	8.4	9.4	8.5

pared the results with our experimental findings. It will become clearer later that this comparison seems to exclude the boiling mechanism.

In this section we will present the results predicted by both models. The thermophysical properties used in the calculations are given in the Appendix, together with some details of the calculational procedure.

The main features of the calculated transients for both models are shown in Table II. One can notice that no significant evaporation takes place for both processes when the energy density is below 3 J/cm^2. In fact, in this case the surface temperature is below T_b and the two models are identical. Above 3 J/cm^2 one finds that for both models many characteristic quantities remain comparable: depth and duration of the molten phase, resolidification velocity, and maximum temperature gradient. The main difference is, of course, the maximum surface temperature which is very high in the thermodynamical-surface-vaporization model. Also the amount of lost material and the duration of the loss stage are very different since in the boiling model a material loss five times larger and occurring in a period about two times smaller than in the thermodynamical evaporation model is predicted.

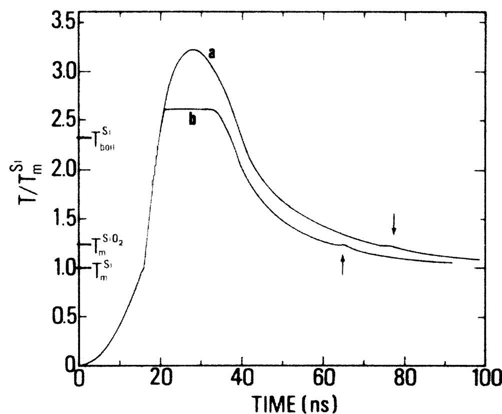

FIG. 8. Time evolution of the *near* surface temperature calculated for an ambient pressure of 4 atm with the thermodynamical surface evaporation (a) and the boiling model (b). T_m^{Si} and $T_m^{SiO_2}$ represent the melting temperatures of Si and SiO_2, respectively. T_{boil}^{Si} is the Si boiling temperature at 1 atm. The arrows point to the small kinks originated during cooling by the resolidification of a 50-nm-thick SiO_2 layer.

These differences will be of crucial importance when comparing the calculations with the experimental results. Another important point is that in both cases the duration of the loss transient is much shorter than the duration of the molten phase. In Fig. 8 we compare the time evolution of the surface temperature in the first hundred nanoseconds for the two models at 3.5 J/cm^2 and the external pressure $P=4$ atm. One can notice that in both cases the boiling temperature is reached, and hence a significant loss can take place, about 3 ns after melting.

V. DISCUSSION

A. Material loss mechanism: Boiling or thermodynamical evaporation?

As seen in Sec. IV the expected material loss amount, when significant, depends drastically on the hypothesis adopted, i.e., boiling or thermodynamical evaporation. As a matter of fact, the time intervals involved are very short (≈ 20 ns) and the thickness of the layer in which boiling can occur is in any case very small (≈ 100 nm) since the molten depth at this time of the transient is about 500 nm and only the near-surface region shows the superheating needed for bubble nucleation. The occurrence of boiling is then questionable since appreciable bubble nucleation seems rather unlikely. In fact, the minimum size, r_{min} of

the gas bubble whose preexistence is a necessary condition in order to start the boiling process, is (Ref. 18)

$$r_{\min}=\frac{2\sigma(T)}{P}\frac{1}{\exp[(T-T_b)MH_{\text{vap}}/k_B T_b T]-1}, \tag{4}$$

where the surface tension is $\sigma(T)=\sigma(T_m)+(d\sigma/dT)(T-T_m)$. Putting in Eq. (4) $T=5000$ K, $P=4$ atm, $MH_{\text{vap}}=4$ eV, $d\sigma/dT=-0.13$ dyn/cm K, and $\sigma(T_m)=865$ dyn/cm (Ref. 19), one obtains $r_{\min}\approx 200$ nm, that is, a radius much higher than the thickness in which the boiling temperature is reached. However, we will, in a first step, assume that boiling is possible and check if it is consistent with our experimental observations.

The results reported in Table II indicate that the amount of silicon loss caused by boiling is about 31 nm, in the case of a pure silicon sample irradiated with a 3.5-J/cm^2 fluence under an ambient pressure of 4 atm. At 1 atm the same calculation predicts a 50-nm material loss because the boiling temperature is an increasing function of the pressure [see Eq. (A3) in the Appendix]. In our "low-pressure" condition (10^{-2} Torr) the loss is expected to be appreciably higher; moreover, the mean-free path of the expelled silicon atoms is large enough to prevent any thermalization or silicon redeposition. In such a situation the material loss can be estimated to be on the order of 10% of the molten quantity.

In our irradiation at low pressure of samples covered by a thin (7 nm) ^{18}O oxide the oxygen loss does not reach 10%. We could assume that in the very short time (≈ 3 ns) between melting and boiling the oxide layer has been diluted uniformly in the whole melted layer. This would imply a surprisingly efficient transport mechanism acting at least over several hundreds of nanometers during the times involved.

Let us assume, for the moment, that it is possible. If we assume that such an efficient transport mechanism is possible the oxide concentration in the melted film would be below 10% even for our thicker oxide films, so that the temperature transients computed for pure silicon could still be used. In this situation, since the oxygen is uniformly distributed over the whole pool, the ^{18}O loss is expected to be a constant and a small fraction of the initial value. This is in strong contradiction with the results reported in Table I (note that in this table the only significant parameter for the present discussion is the remaining ^{18}O quantity, the ^{16}O content resulting from a balance between loss and gain processes). The conclusion is that the boiling mechanism is inconsistent with our experimental results.

We will now verify that thermodynamical evaporation may explain our experimental observations; in fact, as already remarked above, calculations performed within this model estimate an amount of material loss about six times smaller and an evaporation time about two times higher than the corresponding ones computed in the boiling model. These facts imply that the transport mechanism to be invoked in order to explain our ^{18}O results can then be less efficient than that assumed within the framework of a boiling model. This by itself favors the thermodynamical evaporation description.

The transport of the thin oxide film through about 50 nm in 10 ns would be sufficient to prevent most of the film evaporation but will leave a very high SiO_2 concentration in the surface region in the case of thicker oxides. For these oxides the material losses calculated for pure silicon do not apply and one has to take into account the thermodynamical properties of SiO_2. This has been performed for a silicon sample covered by a SiO_2 layer (see Sec. 2 of the Appendix) in the case of thermodynamical evaporation. We found that SiO_2 losses are 28 and 41 nm for laser fluences of 3.5 and 3.8 J/cm^2, respectively. These values compare very favorably with the experimental results reported in Table I, taking into account our 5% uncertainty on laser fluence.

As a conclusion, our experiments seem to discriminate in favor of a thermodynamical evaporation mechanism.

B. Oxygen uptake mechanism

1. Gas or liquid phase reaction?

One could, in principle, imagine that evaporated silicon, with high translational energy, reacts very efficiently with the molecules of the ambient gas and that, because of trajectory randomization in the high-pressure gas phase, half of the reacted species would be redeposited on the sample. This, however, cannot explain the very important oxygen uptake which is measured. In fact, assuming that the thermodynamical evaporation mechanism holds, the number of silicon atoms suitable to react with oxygen in the gas phase to produce SiO_2 could be estimated from Table II. Even assuming a 100% efficiency for the reaction, it is clear that at laser fluences of 3.5 J/cm^2, the maximum oxide thickness attainable would be ten times smaller than that observed, which is on the order of 50 nm, Moreover, the results of Table II indicate that the Si loss is an increasing function of the fluence so that the oxygen content above threshold should also increase with the energy density. This is not the experimental behavior and a reaction of the ambient gas with molten silicon remains the only possibility.

Two conditions must be fulfilled for such a reaction in order to lead to an oxygen incorporation consistent with our experimental results: (i) the number of molecules from the gas hitting the sample surface, while molten, must be greater than the incorporated quantity, and (ii) efficient oxygen (or oxide) transport must take place.

We have already indicated that such a transport is required to interpret all our results, even those related to oxygen losses. The transport mechanism will be discussed in Sec. V B 2. Here we only want to point out that transport is also necessary for condition (i).

In fact, the effect of the transport mechanism will be to maintain a nearly "clean" Si surface layer during most of the time during which the incorporation takes place, by diluting the surface oxide and supplying new free silicon atoms to the surface. Consequently, the melting temperature of this layer would approximately be that of silicon and the corresponding melting time is given in Table II (>500 ns). In such a time the number of gas molecules colliding with the surface is noticeably greater than the

oxygen uptake, even for pressures at which there is no uptake saturation. If there were no efficient transport mechanism, the surface would be very quickly saturated with oxide and it would tend to solidify in a time which is much earlier (<60 ns) than that appropriate in pure silicon (see Fig. 8).

2. *Transport mechanism*

As already stated, an efficient mass transfer must hold both to prevent ^{18}O loss, in the case of thin oxide films, and to explain the ^{16}O incorporation. Such a mechanism can be either diffusion in liquid silicon (or SiO_2) or some kind of hydrodynamical transport (convection).

The results for ^{18}O loss in the 7-nm films irradiated under vacuum conditions, as well as those in the sandwiched $Si\,^{16}O_2/Si\,^{18}O_2$ film seem to be inconsistent with a thermal diffusion transport process. In fact, if one considers that the mixing depth must be at least 50 nm and that the loss characteristic time is 10 ns (see Sec. V A), a diffusion coefficient for oxygen in liquid silicon of the order of 10^{-3} cm^2/sec should be used. Even though we are dealing with very high temperatures, this value seems to be unrealistic if compared with most of the reported values for diffusion coefficients of oxygen in liquid silicon.

The hypothesis of convective motions due to instabilities in the liquid layer, originated both by temperature and oxygen concentration gradients, can explain the very efficient ^{18}O transport observed. The hypothesis of convective material transport during pulse laser irradiation has already been proposed in Refs. 20–22 in which pictures of surfaces showing cellular structures, interpreted as flow patterns frozen during solidification, have been presented.

As to the type of convection mechanism, it must be remembered that the nature of the instability depends on the liquid-layer thickness.[23] In fact, in thick layers the decisive factor is the buoyancy force, in thin layers ($h \leq 1$ mm) the thermocapillarity is predominant. The driving force of this mechanism is originated by the surface-tension gradients (Marangoni effect): lateral variation of surface tension can be generated by fluctuations in temperature as well as by fluctuations in the absorption of surfactive material and by the deformability of the free surface; the last effect is particularly significant for very thin layers of highly viscous liquids.[23] Moreover, the thermocapillarity effect is a threshold mechanism[23] entirely independent of the direction of gravity, and it can produce cellular motions in thin liquid films covering surfaces at an arbitrary inclination with respect to the force of gravity. These motions have been observed in shallow pools heated from above[24] and more recently in experiments performed by astronauts in the Apollo 14 and Apollo 17 spacecrafts where the gravitational acceleration was 10^{-6} G. At present we do not make hypotheses on the actual mechanism producing the surface-tension gradients, we only notice that in laser annealing experiments the liquid film is generally thinner than 1 μm; lateral temperature gradients are likely to occur as well because of the evaporation of the surface oxide (native or grown), which certainly produces gradients in the oxygen concentration, as because of surface deformation and hot spots in the laser beam. For these reasons we are oriented to identify the thermocapillarity as the most-likely mechanism sustaining the convective flow in the molten layer once the initial perturbation has started.

The existence of convective motions during the laser pulse may explain the experimental data only if the characteristic time for the onset of such a motion is very short, at most a few nanoseconds. A first rough evaluation of the characteristic time necessary to transfer a surface layer to a depth d can be easily done. In the case of the Marangoni convection the characteristic time is[25]

$$t_c = d\left[\frac{\rho_L \eta}{L}\right]^{1/3} \Big/ \left|\frac{d\sigma}{dT}\frac{\partial T}{\partial x}\right|^{2/3}, \qquad (5)$$

Where η is the viscosity, T, x, and L the temperature, spatial coordinate (normal to the surface) and thickness of the molten pool, respectively. In this case t_c is proportional to $\eta^{1/3}$ and inversely proportional to the $\frac{2}{3}$ power of the temperature gradient. These dependences make the capillarity-driven convection very attractive for our interpretation. In any case, this model yields $t_c \approx 1$ ns with a thermal gradient on the order of 10^7 K/cm (see Table II).

As a partial conclusion, the experimental conditions occurring in this work (high temperature gradients and surface nonhomogeneities) support the assumption of the onset of convective motions having characteristic times short enough to explain the ^{18}O-tracing experiments.

Of course, the mass transport implied by convective motions involves a heat transfer which alters the heat flow of a slowly heated liquid. In any case, the results from the simple heat-flow-model calculation are useful both to assess the onset of conditions favorable to convective motions during a given transient and to give consistency limits to any modelization of a convective process during the transient itself.

3. *Roughness*

The low roughness exhibited by the preoxidized samples, when irradiated with energy densities which are below incorporation threshold, but markedly above the threshold required to melt Si and SiO_2 [see Fig. 7(a)], demonstrates that the sample morphology above threshold cannot be attributed to cracking of the oxide layer, in connection with the quite different thermal expansion coefficient of SiO_2 and Si. As a matter of fact, cracks may appear in some regions, but they represent a negligible part of the surface and do not account for the roughness. Moreover, the very similar and rough surface morphology observed above the 3-J/cm^2 energy-density threshold, whatever is the ambient atmosphere, demonstrates that incorporation is not responsible for this morphology.

As to the mechanisms which produce such a roughness, one has to stress that any evaporation or boiling process has little bearance on it, since as calculations show they are confined to the very early stage of a much longer transient, during which the surface layer remains molten. The observed structure must be related to the physical processes occurring in the last part of the transient in the liquid phase, e.g., the convective processes suggested above to ex-

plain our results. As a matter of fact, it is interesting to notice that the silicon Prandtl number $\eta c/K_L$ (c being the specific heat) (Ref. 26) is rather low (about 2×10^{-2}). Since, among other things, this number gives the square of the ratio between the speed of propagation of the velocity front and that of the thermal front,[27] such a low value seems to favor *instant* freezing of the turbulent mass motion. This should lead to a swelling on the order of the molten thickness, i.e., 1 μm, which is indeed what is experimentally observed.

C. Phenomenological modelization

Before discussing the experimental results we must remember that RBS and nuclear reaction techniques allow thickness measurement in atoms/cm^2 units and these are the units for the thicknesses we have used. Sometimes we will refer to linear units only for the sake of simplicity.

The oxygen content of the silicon samples after laser irradiation is the result of a balance between material loss during the very short time when evaporation is effective ($\approx$20 ns) and incorporation of molecules from the gas during a much longer time. A good approximation will then consist in neglecting the oxygen pickup during evaporation and in treating the loss and the incorporation processes separately. For both processes we will assume that material transport takes place in the molten layer, and calling $x(t)$ the oxygen content (atoms/cm^2) at time t we will consider that the fraction $f(t)$ of the surface covered by oxygen is given by

$$f(t)=\begin{cases}\gamma x^n(t) & \text{if } x^n(t)<\gamma^{-1},\\ 1 & \text{if } x^n(t)\geq\gamma^{-1}=x_s^n.\end{cases} \tag{6}$$

The relation between $f(t)$ and $x(t)$ clearly depends on the nature of material transport mechanism, and, as we cannot reach any direct knowledge about, for instance, the geometry of the convective process, n can be considered here as a fitting parameter. When $x(t)\geq\gamma^{-1/n}=x_s$ the transport is not efficient enough to supply pure Si atoms to the surface from below and the surface layer is a pure oxide. We shall assume that in this situation no oxygen incorporation is possible; x_s is then the maximum oxide thickness that can be obtained after a single pulse irradiation.

1. *Oxygen loss*

If the initial oxide film is markedly thicker than x_s, the surface can well remain covered with oxide during all the evaporation process ($f=1$). Then the oxygen loss is governed by the differential equation

$$dx=-\beta(t)dt\,, \tag{7}$$

where $\beta(t)$ is the evaporation speed at time t, i.e., at temperature $T(t)$, and finally

$$x=x_0-\int\beta(t)dt=x_0-\bar{\beta}t_{ev}\,, \tag{8}$$

where x_0 is the initial oxide thickness, $\bar{\beta}$ is an average evaporation speed which depends on the choice of t_{ev}. For instance, $\bar{\beta}$ could be defined by taking t_{ev} as the time during which the surface temperature is above the boiling point of SiO_2. In any case, the quantity $\bar{\beta}t_{ev}$, i.e., the SiO_2 loss for a Si sample covered by a thick SiO_2 layer has been calculated as indicated in the Appendix.

Let us now consider an initial oxide with thickness $x_0<x_s$. The corresponding differential equation for oxygen loss is

$$dx=-\beta(x,t)f(t)dt\ . \tag{9}$$

In this general form Eq. (9) cannot be easily integrated. However, when comparing the computer calculations for temperature transients in pure silicon and in silicon covered by a thick SiO_2 layer, one realizes that they are very close to each other. This is due to the fact that the amount of energy dissipated in the evaporation process is always small when compared to the total deposited energy. Since β is directly proportional to the evaporation probability of an SiO_2 molecule, which depends only on the surface temperature T, and since the transient $T(t)$ can be considered as being independent of x, $\beta(x,t)$ can be considered as a function of the parameter t only. Under this assumption Eq. (9) can be rewritten as

$$dx=-\beta(t)\gamma x^n dt\ . \tag{10}$$

Clearly for $n=1$, dx is proportional to x and the relative loss is independent of the film thickness. This is the value for n that was used in Ref. 12, where all the data about oxygen loss were not yet available and it is in contradiction with the results of Table I where we have noticed that the thicker oxides loose, in proportion, much more than the thinner ones. As the present model is mostly phenomenological, we have not attempted to use the value of n which would give the best fit to our experimental data: a fair agreement may be obtained with the simple value $n=2$ and we have adopted this value. Then one obtains

$$x=\frac{x_0}{1+x_0\gamma\bar{\beta}t_{ev}}\,, \tag{11}$$

$\bar{\beta}t_{ev}$ is the same as in relation (8) and we have taken the value $\bar{\beta}t_{ev}=41$ nm (see end of Sec. V A). We also have the experimental datum $x_s=\gamma^{-1/2}=245\times10^{15}$ O/cm^2 $\approx$56 nm.

Equation (11) is valid for initial thicknesses smaller than x_s and we can use it to compute the losses on 7- and 41-nm oxides and to compare them with the measurements. For these thicknesses Eq. (11) gives, respectively, losses of 8% and 35% instead of 10% and 56% experimentally found, i.e., a fair agreement.

For oxides thicker than x_s like the 69-nm oxide layer, also experimentally studied, the evaporation proceeds in two stages: (i) as far as $x(t)$ is greater than x_s, it is governed by Eq. (7); (ii) when, because of evaporation, x becomes smaller than x_s, it becomes governed by Eq. (10). In any case, provided that the final oxide thickness after evaporation is smaller than x_s, the evaporated fraction is an increasing function of the initial thickness: this is the behavior experimentally observed. When the remaining thickness after evaporation is greater than x_s, the overall evaporation process is governed by (8) and the maximum

evaporated quantity for laser fluences around 3.8 J/cm^2 is of the order of 40 nm.

2. Oxygen pickup

After a time of the order of t_{ev} the evaporation stops and we are left with a remaining oxygen content that we will call x'_0. If $x'_0 < x_s$ oxygen pickup from the gas phase may take place. We shall assume that each oxygen molecule impinging on a free silicon atom at the surface has a sticking coefficient close to 1. At time t, the incorporation rate is hence given by

$$dx = \begin{cases} \nu\alpha P[1-f(t)]dt & \text{if } f(t)<1, \\ 0 & \text{if } f(t)=1, \end{cases} \tag{12}$$

where $1-f(t)$ is the oxygen-free surface fraction, P is the gas pressure and, $\alpha=(2\pi M k_B T)^{-1/2}$, αP being then the impinging rate of the gas molecules per surface unit area, and ν is the number of atoms per molecule available for the reaction, for instance $\nu=2$ in the O_2 case.

By using Eq. (6) with $n=2$, the integration of Eq. (12) yields the final oxide thickness x_f after laser irradiation:

$$x_f = x_s \frac{A\exp(2\nu\alpha P t_{\max}/x_s)-1}{A\exp(2\nu\alpha P t_{\max}/x_s)+1}, \tag{13}$$

where x_f and x_s are experimentally determined and

$$A = \frac{x_s + x'_0}{x_s - x'_0}, \tag{14}$$

with x'_0 given by Eq. (11) for not-too-thick initial oxides. As a matter of fact, we use $x'_0 = 25\times10^{15}$ O/cm^2, this value being the experimental oxygen content of a sample irradiated in "vacuum." Thus the only free parameter in Eq. (13) is $t_{\max}$, i.e., the time during which convection is effective after evaporation stops. This characteristic time can be easily evaluated by the initial slope of the x_f-versus-P curve, which is given by

$$\left[\frac{dx}{dP}\right]_{P=0} = \frac{x_s^2 - x_0'^2}{x_s^2}\nu\alpha t_{\max} \approx \nu\alpha t_{\max}. \tag{15}$$

However, in order to improve our accuracy, we used $t_{\max}$ as a fitting parameter to *all* the experimental points. The resulting best fit is presented in Fig. 4. It is obtained for a value $t_{\max}=148$ ns, i.e., six times smaller than the time during which the surface remains molten. Note however that $t_{\max} \gg t_{ev}$ and that, consequently, our treatment, which neglects oxygen pickup during evaporation, is a good approximation. It must also be noted that in Ref. 12, by using $n=1$ in Eq. (6), we obtained $t_{\max}=180$ ns. This comparison suggest that our estimate of $t_{\max}$ is not strongly dependent on the value assumed for n, a value which is not known at present.

3. Case of CO_2 atmosphere

In the model described above we have assumed that the ambient atmosphere was O_2. We have now to understand why, in the case of CO_2 ambient, the slope for oxygen pickup is two times smaller at small pressures and why the saturation of the pickup occurs in the same pressure range as for O_2 but with a value for x_s one-half smaller (see Fig. 4). As already said in Sec. III B and discussed in Ref. 12, the probability that a given reaction between silicon atoms and the gas ambient molecules takes place, seems to be better described in terms of the "bond strength" of the reactants and of the products—that is, by the heat of the reaction—than by the heat of formation of the final compounds. In this scheme a CO_2 molecule impinging on a free silicon atom reacts giving SiO + CO and the CO remaining compound is not able to react further. This picture accounts for the slope of oxygen pickup as a function of pressure; in fact, in this case $\nu=1$, and the value of $\nu\alpha$ for CO_2 ambient gas is then about one-half the corresponding one for O_2: for a given $t_{\max}$ Eq. (15) gives a slope two times smaller for CO_2 than for O_2 ambients.

The difference in the saturation level x_s is more difficult to explain, because in our model it is only related to the efficiency of the transport mechanism in supplying Si atoms to the surface. In this view the different CO_2 saturation level can only be explained with a more-efficient coverage of the surface. This could be obtained by two different mechanisms:

(i) Once an SiO molecule is formed, the reactions

$$SiO + CO_2 \rightarrow SiO_2 + CO \tag{16}$$

and

$$SiO + SiO \rightarrow SiO_2 + Si, \tag{17}$$

even though energetically possible, do not take place during the convective motions for some as yet unclear reasons. Consequently, the oxygen pickup stops when convection is no more able to prevent the formation of a saturated SiO surface layer. This would lead to one-half of the oxygen pickup corresponding to a saturated SiO_2 layer. Because even in the CO_2 case we observe the formation of an SiO_2 surface layer, the reaction (17) should take place during the resolidification;

(ii) Both reactions (16) and (17) can take place during the convective process, so that the surface should be saturated by SiO_2. The only way to explain the lower saturation value is then admitting that the nonreacting CO molecules are incorporated in the liquid film and that the oxygen incorporation stops when only one-half of the surface is covered by SiO_2, the remaining part being protected by a CO coverage. The CO molecules, which do not react, would then be expelled during the resolidification process.

In our opinion, none of these mechanisms seems to be satisfactory and we take both x_s values, i.e., for O_2 and for CO_2, as experimental data. It must be stressed that by fitting Eq. (13) to the experimental data, the $t_{\max}$ parameter is strongly dependent on the assumed x_s value. As a consequence the most important result is that we obtain an excellent fit to the CO_2 data by using the same $t_{\max}$ value as for the O_2 case (see Fig. 4). This fact is highly satisfactory because it implies that the transport mechanism is not affected by the gas ambient and gives further consistency to our modelization.

VI. CONCLUSION

The present work provides information both on loss and incorporation mechanisms during high-fluence pulsed-laser irradiation under reactive ambient atmospheres. The experiments were relative to silicon in an oxidizing gas ambient. In this situation we observed that for single-pulse irradiations significant incorporation may take place (50-nm surface oxide are formed) but only for laser fluences at which important material losses also occur. The amount of material loss could be measured in the case of preoxidized samples and these measurements have allowed us to discriminate between various loss mechanisms. It appears that the most simple and natural mechanism, i.e., thermodynamical evaporation can account for all our experimental results. The consideration of different loss mechanisms such as "laser sputtering" which have been invoked by some authors[6] never appeared necessary here.

The coincidence between the energy threshold for significant evaporation and incorporation could give some support to the hypothesis that incorporation is related to the reaction of vaporized atoms with molecules from the ambient gas, some of the reacted species being redeposited onto the sample. We show that in our case, this seems not to be the major process as the corresponding incorporation should be much smaller than that experimentally observed; hence the reaction has to take place in the liquid phase. However, the coincidence between significant evaporation and incorporation threshold is not fortuitous. The liquid-phase process requires an efficient transport mechanism inside the liquid film of the incorporated species in order to provide the surface with oxygen-free silicon atoms able to react with the gas molecules. We have experimentally evidenced, by using ^{18}O-tracing experiments, that such a transport does take place. We have also shown that this transport is so efficient that it cannot simply be due to diffusion in the liquid phase; convective transport was then assumed. The role of significant evaporation would then be to introduce surface-tension gradients which could be the driving force for the convection. We have proposed a phenomenological model in order to fit our experimental results relative to the dependence of the incorporated amount on the ambient pressure. In particular, we had to account for the incorporation saturation at high pressures. In our model we attribute this saturation to the efficiency of the convective process. From our model we derive information about the time during which convection is effective. This time (≈ 150 ns) is significantly smaller than the duration of the molten phase and it is not strongly dependent on the particular geometry of the convective motion. Finally, we have also interpreted the difference of the oxygen pickup rate under O_2 and CO_2 ambient atmospheres. This difference can be accounted for by considering that a chemical reaction between the gas ambient molecules and the molten silicon must take place at the surface to ensure the final incorporation and by taking into account that these reactions are governed by a balance of the bond strengths. For this reason the number of oxygen atoms per impinging molecule reacting with silicon can be lower than the number of oxygen atoms in the gas molecule.

Finally, we have to note that the surface roughness of the oxides is very high and that such a fact seems to be due to a memory of the convective process.

APPENDIX

1. Calculational procedure for evaporation and boiling

In order to solve the one-dimensional heat-flow equation with a finite difference method and taking into account the boundary conditions describing the material loss (either as evaporation or boiling off) at the surface, we consider a grid whose points are partly moving and partly fixed according to the following specifications. The grid is made of three sets of points in an ordered sequence. A first set contains ten points, which are equally spaced and whose spacing shrinks at each time step in a way which is proportional to the amount of material lost at the surface at the end of the previous time step. When the total lost thickness equals the initial spacing Δx (e.g., $\Delta x = 50$ nm), the first point of the moving mesh is removed and the spacing between the remaining points restored to its initial value; then shrinking goes on, etc., as long as the loss mechanism is at work. The second and third set contains only fixed points, 150 and 40 points, respectively; their spacing is equal to Δx and $10\Delta x$, respectively, in order to calculate the heat flux with sufficient details in the near surface region and to reach a depth in the bulk, where the temperature equals that of the external thermal bath.

In general, on each point of the grid, the time derivative of the temperature $T(x,t)$ is

$$\frac{dT}{dt} = \frac{\partial T}{\partial t} + \frac{\partial T}{\partial x}\dot{x} , \tag{A1}$$

where $\dot{x}$ is the speed along the x axis of the given point.

The heat-diffusion equation then becomes

$$\rho c \frac{dT}{dt} = \frac{\partial}{\partial x}\left[K \frac{\partial T}{\partial x} \right] + \rho c \frac{\partial T}{\partial x}\dot{x} + Q(x,t) , \tag{A2}$$

where $Q(x,t)$ is the source term and c is the specific heat.

Equation (A2) can be discretized, provided that $\dot{x}$ is known at each point. As a matter of fact, $\dot{x}$ is simply related, by means of the above shrinking grid hypothesis, to $\dot{S}$, the speed of the moving surface front. In the case of the thermodynamical evaporation model, $\dot{S}$ is given by Eq. (2), as a function of the initial temperature of the first grid point at each time step. In the case of the boiling-off model, $\dot{S}$ is determined in the following way. Let us discretize Eq. (A2) and consider the situation at the first grid point when $T = T_b$. First of all, $dT/dt = 0$; moreover, the first term at the right-hand side can be discretized according to

$$\frac{\partial}{\partial x}\left[K \frac{\partial T}{\partial x} \right] = \left[-\Phi_s + K_{1,i} \frac{T_{2,i} - T_{1,i}}{\Delta x_i} \right] \Big/ x_i ,$$

where the index i refers to the previous time step and where 1 and 2 refer to the first and second grid point, respectively; Φ_s, i.e., the heat flux from the surface, is equal to $\rho_L H_{\rm vap} \dot{S}$, the speed $\dot{S}$ being an as yet unknown quantity; finally, $\dot{x}_1$ is simply proportional (almost equal)

to $\dot{S}$, according to the shrinking-grid assumption. Then, as a conclusion, Eq. (A2), when discretized and applied to the first grid point (at $T=T_b$), yields the condition required to calculate $\dot{S}$, and hence the speed of the other moving grid points, the shrinking to be used in the subsequent time step and so on. Further details, together with consistency tests, will be given in a forthcoming paper.

2. Computational details and thermophysical parameters used in the calculation

The space mesh has steps 50-nm long (or less in the near surface region, see Sec. 1 of this appendix), the time step being determined by the usual convergence condition.

At pulse energy densities E_p just above the Si-melting threshold, the energy deposition occurs both in solid and in liquid phase. Accordingly we assumed that the optical reflectivity R and the absorption length α^{-1} vary from their value $R_c=0.35$ and $\alpha_c^{-1}=2000$ nm (Ref. 28) in the crystalline solid phase to the values $R_L=0.7$ (Ref. 29), $\alpha_L^{-1}=30$ nm (Ref. 30) corresponding to the almost metallic optical properties of liquid silicon. As to the thermodynamical data governing the heat flow in silicon, we use for the density and specific heat (both in liquid and solid phases), respectively, $\rho=2.33$ g/cm^3, $c=0.95$ J/g; for the thermal conductivity in the solid phase we use $K_S(T)=1.35(300/T)^{1.12}$ W/cm K (Ref. 31) and in the liquid phase we use $K_L=1.5$ W/cm K (as to K_L, a still uncertain quantity,[32] notice that when calculations were carried out with lower K_L values, down to 0.5 W/cm K, they gave substantially equal results). The melting and boiling temperatures were taken to be $T_m=1412\,^{\circ}\mathrm{C}$ and $T_b=3270\,^{\circ}\mathrm{C}$ at 1 atm, respectively.[33] The boiling temperature $T_b(P)$ was assumed to vary with the ambient pressure P according to the following equation:[17]

$$P=P_0\exp\left[\frac{MH_{\mathrm{vap}}}{k_B T_b}\left[1-\frac{T_b}{T_b(P)}\right]\right], \qquad \text{(A3)}$$

where $P_0=1$ atm and $MH_{\mathrm{vap}}=4$ eV is the evaporation latent heat per atom; notice that T_b in Eq. (A3) must be expressed in Kelvin degrees. The macroscopic melting and evaporation latent heats are, respectively, 1790 and 13 700 J/g.[33] Finally, in order to take into account possible delaying effects during the cooling stage due to the presence of a reacted SiO_2 layer at the surface of the sample, we changed the resolidification temperature and the latent heat in a surface layer about 50-nm-thick from those of pure crystalline silicon to those pertaining to SiO_2, i.e., 1725 °C and 146.5 J/g, respectively,[34] the other thermodynamic quantities being equal to the silicon ones. Calculations show that such a change does not yield appreciable modifications in the overall thermal transient.

Finally, in some calculations concerning samples covered with thick oxide layers we used for silica a latent heat value of 7080 J/g and a boiling temperature of 2108 °C [derived through Eq. (A3) from vapor pressure data[35]], the other thermodynamical quantities being again equal to the silicon ones.

ACKNOWLEDGMENTS

The authors wish to thank F. Rochet for the preparation of the Si $^{16}O_2$/Si $^{18}O_2$/Si samples and M. von Allmen for information and discussions on the thermophysical parameters of Si. Work partially supported by the Italian Ministero della Pubblica Istruzione (MPI)-40% research fund, by the twin European Economic Communities (EEC) Contract No. STI-043-J-C (CD) and by the French Centre National de la Recherche Scientifique (CNRS) within Groupement de Recherches Coordonnées (GRECO) No. 86.

[1]K. Hoh, H. Koyama, K. Uda, and Y. Miura, Jpn. J. Appl. Phys. **19**, L375 (1980).

[2]M. Matsuura, M. Ishida, A. Suzuki, and K. Hara, Jpn. J. Appl. Phys. **20**, L726 (1981).

[3]G. B. Turner, D. Tarrant, G. Pollock, R. Pressley, and R. Press, Appl. Phys. Lett. **34**, 967 (1981).

[4]C. Cohen, J. Siejka, M. Berti, A. V. Drigo, G. G. Bentini, D. Pribat, and E. Jannitti, J. Appl. Phys. **55**, 4081 (1984); J. Phys. (Paris) Colloq. **C1-43**, 229 (1982); J. Phys. (Paris) Colloq. **C5-44**, 179 (1983).

[5]T. E. Orlowski and H. Richter, Appl. Phys. Lett. **45**, 241 (1984).

[6]R. Kelly and J. E. Rothenberg, Nucl. Instrum. Methods B **7/8**, 755 (1985).

[7]Y. S. Liu, S. W. Chiang, and W. Katz, Mat. Res. Soc. Symp. Proc. **4**, 249 (1982).

[8]See, e.g., P. Baeri, Mat. Res. Soc. Symp. Proc. **4**, 151 (1982), and references therein.

[9]G. Herziger and E. W. Kreutz, in *Laser Processing and Diagnostics*, Vol. 39 of *Springer Series in Chemical Physics*, edited by D. Bäuerle (Springer-Verlag, Berlin, 1984), p. 90.

[10]M. J. Bedzyc and W. M. Gibson, Vac. Sci. Tech. **20**, 634 (1982).

[11]E. Rosencher, A. Straboni, S. Rigo, and G. Amsel, Appl. Phys. Lett. **34**, 254 (1979).

[12]M. Berti, A. V. Drigo, G. G. Bentini, C. Cohen, J. Siejka, and E. Jannitti, in *Energy Beam—Solid Interactions and Transient Thermal Processing*, edited by V. T. Nguyen and A. G. Cullis (les Editions de Physique, Paris, 1985), p. 131.

[13]L. F. Doná dalle Rose and A. Miotello, Radiat. Effects **53**, 7 (1980).

[14]A. Miotello and L. F. Doná dalle Rose, Phys. Lett. **98A**, 367 (1983).

[15]L. F. Doná dalle Rose, J. Phys. (Paris) Colloq. **C5-44**, 469 (1983).

[16]F. V. Bunkin and M. J. Tribel'skii, Usp. Fiz. Nauk **130**, 193 (1980) [Sov. Phys.—Usp. **23**, 105 (1980)].

[17]V. A. Batanov, F. V. Bunkin, A. M. Prokhoorov, and V. E. Fedorov, Zh. Eksp. Teor. Fiz. **63**, 586 (1972) [Sov. Phys.—JETP **36**, 311 (1973)]; see also J. F. Ready, J. Appl. Phys. **36**, 462 (1965).

[18]J. Frenkel, *Kinetic Theory of Liquids* (Dover, New York, 1955), p. 373.

[19]A. V. Grosse, J. Inorg. Chem. **22**, 23 (1961); and E. T. Turk-

dogan, *Physical Chemistry of High Temperature Technology* (Academic, New York, 1980), pp. 92–94.

[20]G. E. Possin, H. G. Parks, and S. W. Chiang, Mat. Res. Soc. Symp. Proc. **1**, 73 (1981).

[21]L. D. Laude, in *Laser Processing and Diagnostics,* Vol. 39 of *Springer Series in Chemical Physics,* edited by D. Bäuerle (Springer-Verlag, Berlin, 1984), p. 355.

[22]G. G. Bentini, in *Festkörperprobleme (Advances in Solid State Physics),* edited by P. Grosse, (Vieweg, Braunschweig, 1985), Vol. XXV, p. 121.

[23]G. Z. Gherzumi and E. M. Zhirkovitskii, in *Convective Instabilities of Compressive Fluids* (Israel Program for Scientific Translations, Jerusalem, 1976), pp. 245–251.

[24]M. J. Block, Nature **22**, 650 (1956).

[25]D. Schwabe and A. Scharmann, J. Cryst. Growth **52**, 435 (1981).

[26]See, e.g., F. Rosenberger, *Fundamentals of Crystal Growth I,* (Springer-Verlag, New York, 1979).

[27]T. R. Anthony and H. E. Cline, J. Appl. Phys. **48**, 3888 (1977).

[28]G. E. Jellison, Jr., and F. A. Modine, Appl. Phys. Lett. **41**, 180 (1982).

[29]P. S. Peercy and W. R. Wampler, Appl. Phys. Lett. **40**, 768 (1982).

[30]See, e.g., Baeri, Ref. 8, p. 153, where a value equal to ~ 20 nm is reported. The present calculation does not critically depend on the actually chosen value since $\Delta x \sim 50$ nm.

[31]J. R. Meyer, M. R. Kruer, and F. J. Bartoli, J. Appl. Phys. **51**, 5513 (1980).

[32]M. O. Thompson, J. W. Mayer, A. G. Cullis, H. C. Webber, N. G. Chew, J. M. Poate, and D. C. Jacobson, Phys. Rev. Lett. **50**, 896 (1983).

[33]C. J. Smithells, *Metals Reference Book,* 5th ed. (Butterworths, London, 1976).

[34]*Handbook of Chemistry and Physics,* 55th ed., edited by R. C. Weast (Chemical Rubber Co., Cleveland, 1974).

[35]C. J. Smithells, *Metals Reference Book,* 4th ed. (Butterworths, London, 1967), Vol. 1, p. 229.

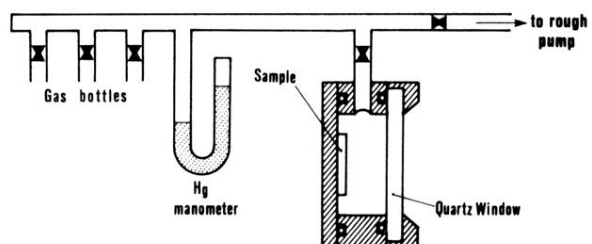

FIG. 1. Schematic drawing of the experimental arrangement. The laser light enters the cell from the right-hand side of the figure.

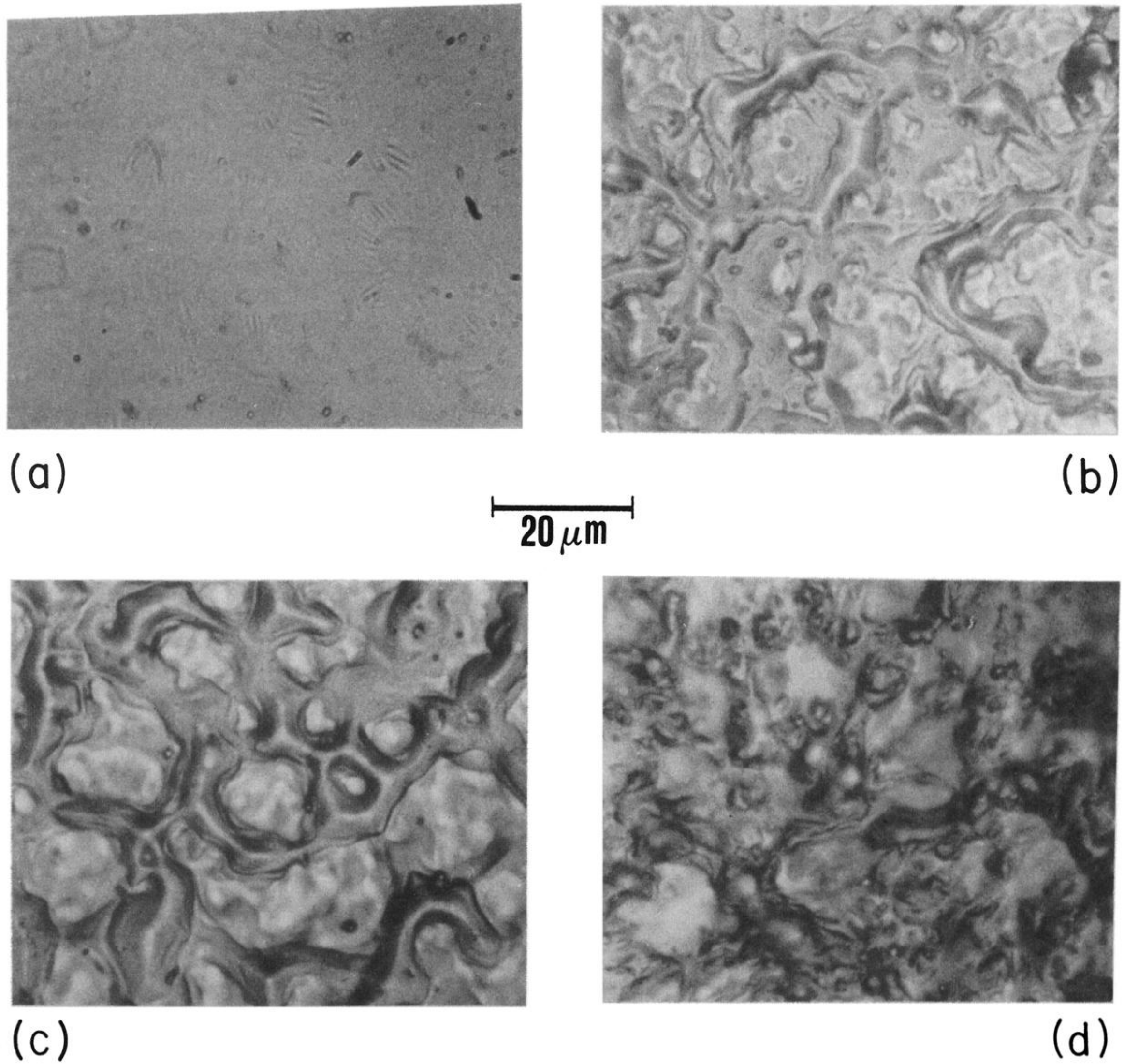

FIG. 7. Optical micrographs of the surface of some selected samples. (a) and (b), 7-nm SiO_2 on Si after 2.3 and 3.5 J/cm^2 irradiation in vaccum, respectively; (c) and (d), Si irradiated at 3.5 J/cm^2 under 2 atm of NH_3 and 4 atm of O_2, respectively.